von Kármán swirling flow between a rotating and a stationary smooth disk: Experiment

Aryesh Mukherjee[1] and Victor Steinberg[1,2]
[1]*Department of Physics of Complex Systems, Weizmann Institute of Science, Rehovot 76100, Israel*
[2]*The Racah Institute of Physics, Hebrew University of Jerusalem, Jerusalem 91904, Israel*

(Received 16 July 2017; published 9 January 2018)

Precise measurements of the torque in a von Kármán swirling flow between a rotating and a stationary smooth disk in three Newtonian fluids with different dynamic viscosities are reported. From these measurements the dependence of the normalized torque, called the friction coefficient, on Re is found to be of the form $C_f = 1.17(\pm 0.03)\mathrm{Re}^{-0.46\pm0.003}$ where the scaling exponent and coefficient are close to that predicted theoretically for an infinite, unshrouded, and smooth rotating disk which follows from an exact similarity solution of the Navier-Stokes equations, obtained by von Kármán. An error analysis shows that deviations from the theory can be partially caused by background errors. Measurements of the azimuthal V_θ and axial velocity profiles along radial and axial directions reveal that the flow core rotates at $V_\theta/r\Omega \simeq 0.22$ (up to $z \approx 4$ cm from the rotating disk and up to $r_0/R \simeq 0.25$ in the radial direction) in spite of the small aspect ratio of the vessel. Thus the friction coefficient shows scaling close to that obtained from the von Kármán exact similarity solution, but the observed rotating core provides evidence of the Batchelor-like solution [Q. J. Mech. Appl. Math. **4**, 29 (1951)] different from the von Kármán [Z. Angew. Math. Mech. **1**, 233 (1921)] or Stewartson [Proc. Camb. Philos. Soc. **49**, 333 (1953)] one.

DOI: 10.1103/PhysRevFluids.3.014102

I. INTRODUCTION

The flow driven by a smooth infinite disk rotating at a constant angular velocity Ω around an axis perpendicular to its plane in an unbounded quiescent fluid was first addressed theoretically by von Kármán [1]. Assuming a self-similar axisymmetric velocity profile, he derived an exact solution to the Navier-Stokes equation in cylindrical coordinates, for a laminar flow driven by a smooth disk rotating with a constant angular velocity Ω in an otherwise resting fluid, by reducing it to a system of two coupled nonlinear ordinary differential equations as a function of only one spatial coordinate, namely, the normalized distance from the disk $z(\Omega\rho/\eta)^{0.5}$ [1], where ρ and η are the density and the dynamic viscosity of the fluid, respectively. Cochran later obtained the first accurate numerical solution of the von Kármán similarity equations, which revealed the three-dimensional flow structure; fluid is drawn in axially toward the rotating disk and thrown out radially, acting as a centrifugal fan [2]. Using results from an infinitely extended disk, one obtains an expression for the dimensionless torque or friction coefficient for a disk of finite radius R much larger than a boundary layer thickness, wetted on both sides,

$$C_f \equiv 2\Gamma/\rho\Omega^2 R^5 = C/\sqrt{\mathrm{Re}}, \tag{1}$$

where $\mathrm{Re} = \rho\Omega R^2/\eta$ is the Reynolds number, $C = 1.935$ [3], Γ is the torque, and R is the disk radius.

A central issue is how well the von Kármán similarity solution approximates the flow between shrouded disks, i.e., between a finite rotating and a stationary disk confined by a cylinder. Several steps have been taken to solve this problem since Bathelor's important paper [4], where he and later on

Stewartson [5] considered a flow between two infinite, concentric, rotating disks as a generalization of the von Kármán problem. In the particular case of flow between infinite rotating and stationary disks, Batchelor predicted that the fluid in the core would rotate with a constant angular velocity of $\sim 0.3\Omega$ and boundary layers would be present at each disk with influx of mass into the boundary layer at the rotating disk and mass efflux from that at the stationary one [4]. Contrary to this result, Stewartson found, using a low-Reynolds-number expansion, that the fluid in the flow core would not rotate but moved axially toward the rotating disk, in agreement with the von Kármán similarity solution [5]. This contradiction between two different self-similar solutions ignited considerable interest of mathematicians and numerical simulation experts in the problem of the existence and uniqueness (or multiplicity) of the solution. The ensuing development in various mathematical approaches and numerical calculations is reviewed in Ref. [6].

Numerical analysis of the flow between two coaxial infinite disks, one rotating and one stationary [7], revealed the problem of multiplicity of similarity solutions. While single-cell solutions such as the Batchelor and Stewartson types were shown to exist, there were many other multiple-cell solutions illustrating that many solutions exist for a given Reynolds number, here defined as $\mathrm{Re} = \rho\Omega H^2/\eta$, where H is the separation distance between the disks. Out of a great number of possible solutions, three solution branches were identified. Among the one-cell solutions two subbranches were found. The first solution existed from zero to infinite Re and was characterized by solid body rotation, i.e., the Batchelor solution, and was also verified in an experiment presented in the same paper [7]. The second tended to the von Kármán or Stewartson solution characterized by a single boundary layer at the rotating disk in the infinite-Re limit.

The similarity solutions discussed so far were also derived for infinitely extended disks without lateral boundary conditions, i.e., unshrouded disks, and their ability to describe the flow between disks of a finite extent with lateral boundary conditions still requires verification. That shrouding the disks strongly affected the flow between the disks was first addressed in Ref. [8], where it was shown that the shrouded configuration showed core rotation as predicted by the Batchelor solution, while the flow in the unshrouded configuration resembled the Stewartson prediction [8]. Measurements of velocity profiles of core rotation that quantitatively agreed with numerical simulations were published in Ref. [9]. To assess the ability of similarity solutions in describing the flow between finite rotating disks one numerical and two extensive experimental studies were conducted [10–12]. Similarity solutions are expected to be applicable when the aspect ratio R/H, where R is the disk radius and H is the disk separation, is large and $s = \Omega_\infty/\Omega = 0$, where Ω_∞ is the angular velocity either at infinity or at the second disk. In an experiment with $R/H \simeq 80$, $s = 0$ and Re in the range between 10^4 and 3×10^5, core rotation, in accord with the Batchelor similarity solution obtained for the flow between infinite disks, was observed up to $r/R = 0.9$, in agreement with numerical simulations [12]. In Ref. [10] a similar experiment at $R/H \simeq 14$ but significantly lower Re up to 1000 also showed core rotation in at least 50% of the radial domain of the fluid outside the disk boundary layers. The relevance of similarity solutions to the flow between the disks of large but finite radius was also studied numerically in Ref. [11]. That work applied an asymptotic analysis to nondimensional equations of motion in the limit of the arbitrary large aspect ratio and showed that the aspect ratio R/H dropped out of all equations and boundary conditions. Using this approach, it can be determined which, if any, of the similarity solutions provide a valid description of the flow between either shrouded or unshrouded rotating disks of a finite extent and over what portion of the radial domain at all axial locations. First, it was found that the effect of the lateral wall grew more prominent with increasing Re and a larger part of the radial domain starting from the wall deviated from the similarity solution, due to propagation of end perturbations toward the center. Second, at $\mathrm{Re} \geqslant 250$, the lateral boundary conditions determined which similarity solution corresponded to the observed flow: The unshrouded flow resembled the Stewartson solution, whereas the shrouded flow was similar to the Batchelor solution [10,11].

Although swirling flow is one of the few examples of exact solutions to the Navier-Stokes equation, experimental studies of the dependence of the friction coefficient C_f on Re are quite sparse. The old data on C_f deviate significantly from the prediction presented in Eq. (1) and only a single set

of the data conducted in air agrees well with the theory in a laminar regime [13]. In this paper we present precise measurements of the friction coefficient C_f of the von Kármán swirling flow between a rotating and a stationary smooth disk in a closed cylindrical vessel with small aspect ratio $R/H \sim 0.55$ for three glycerol-water solutions with a factor of 20 variation in the dynamic viscosity η and a wide range of Re. The friction coefficient C_f exhibits a well-defined scaling relation for all three fluids with Re in the laminar regime and its exponent and coefficient agree with theory and simulations down to $\Omega \approx 2$ rad/s. The experimentally measured ratios of rms torque fluctuations $\Gamma_{\rm rms}$ to the average value Γ for all three fluids are constant $\sim 7 \times 10^{-4}$ and independent of η with small deviations at small Ω due to the growing contribution of measurement errors $\Gamma_{\rm err}$ at small values of Γ. Further, we measured radial and axial profiles of the azimuthal $V_\theta(r,z)$ and axial $V_z(r,z)$ components of the average velocity field using two-velocity-component laser-Doppler velocimetry (LDV).

In total, the flow can be summarized to have four zones. Close to the disk there is a boundary layer which is too thin to be imaged, but at the disk surface the fluid velocity is equal to the disk velocity. Outside the boundary layer there are two regions, inner and outer. The inner region is characterized by solid body rotation, i.e., all fluid elements rotate with the constant normalized angular velocity $\bar{V}_\theta/r\Omega \simeq 0.22$ close to the rotating disk within a normalized radius $r_0/R \simeq 0.25$ until about $z \approx 4$ cm in the laminar regime. It shrinks until $z \approx 11$ cm and rotates with the reduced normalized angular velocity down to $\bar{V}_\theta/r\Omega \simeq 0.19$ and with the reduced core radius $r_0/R \approx 0.19$. Hence the inner region is a solid core that extends from the top to the bottom disk but shrinks considerably down to a point at the stationary disk. In the outer region the angular velocity decreases from the core radius up to the edge of the cylinder and has considerable radial inflow. Finally, there is a fourth region, which is a recirculating layer at the walls of the cylinder, into which fluid is ejected from the disk surface due to centrifugal forces.

II. EXPERIMENTAL SETUP

The apparatus to generate a swirling flow consists of a cylinder made of Lucite (Plexiglas) of diameter $D = 29$ cm and height $L = 31$ cm surrounded by a hexagon-shaped Lucite enclosure with the gap in between filled with water. One 10-mm-thick Lucite smooth disk of $R = 13.2$ cm and $H = 24$ cm apart from the bottom ($R/H = 0.55$) is used as a rotating disk, while the cylinder bottom is used as the stationary one (see Fig. 1). The cylinder is filled with fluid up to the brim such that the rotating disk lies 7 cm below its surface.

A brushless sinusoidal servomotor F-6100 (Electro-Craft servo systems) with a maximum continuous torque of 13 Nm and a peak torque of 31.1 Nm controlled by a motion card PCI-7344NI (Advanced Motion Controls) via optical encoders with proportional-integral-derivative (PID) control that stabilized constant velocity within 0.1% up to $\Omega = 45$ rad/s was used to rotate the Lucite disk and create the experimental flow. Fluid circulating within the hexagonal chamber served as a thermal bath to maintain a desired fluid temperature (stable to within 0.1 °C) which was measured using three thermistors placed at three different heights (2, 20, and 28 cm measured from the top) within the cylinder and a resistance thermometer was used for calibration and the temperature stabilized at the required range $T = 20$ °C–40 °C by three circulating refrigerators (Lauda Inc.). The thermistors extend $l \sim 10$ cm into the bulk of the fluid, but they are thin ($d \approx 1 \times 10^{-3}$ m) compared to the vessel size ($D \approx 0.3$ m). For the range of Re studied in the experiment the drag coefficient is $C_d \equiv F/(1/2)ld\rho U^2 \sim 1$ (see Ref. [13]), so we can estimate the torque due to a thermistor drag $\Gamma_{\rm th} \sim FD/2 \sim C_d(D/4)ld\rho U^2$, where F is the force, U is the fluid velocity (for example, it is $U \sim 0.2$ m/s at 200 rpm, and $\mathrm{Re} = 5 \times 10^4$), and $d \sim 10^{-3}$ m and $l \sim 0.1$ m are the thermistor diameter and length, respectively. Hence $\Gamma_{\rm th} \sim 3 \times 10^{-4}$ Nm, which is smaller than the torque resolution in our experiment 1×10^{-3} Nm and can be neglected. At the smallest rotation velocity 20 rpm, the $\Gamma_{\rm th}$ will be 100 times smaller.

The torque applied on the upper disk to generate the swirling flow was measured by a noncontact calibrated, precise torque meter MCRT No. 48999VB(5-1)NFNN (S. Himmelstein Co.) with a range

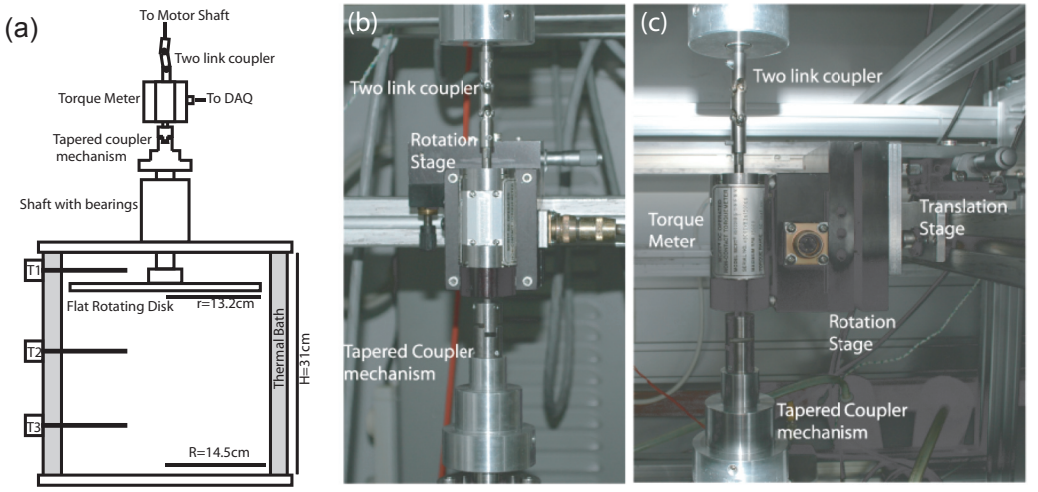

FIG. 1. Experimental setup: (a) schematics, (b) front view of the torque meter arrangement, and (c) side view of the torque meter arrangement.

of 0.35 Nm and overload up to 0.7 Nm with 0.1% of the full scale resolution. It has two low-pass filter outputs: one with a bandwidth between dc and 500 Hz, which we use in the measurements, and another one with the bandwidth between dc and 1 Hz, we used to verify the average value of torque. Output rms noise is 0.1% of the full scale at 500 Hz and 0.01% at 1 Hz. With this highly sensitive torque meter, careful measurements of the background frictional forces resulted in a value of $\sim$3m Nm, an order of magnitude larger than the resolution of the device. This value of the background was measured at $\Omega > 10\,\mathrm{rad/s}$ and was reproducible for different experimental runs. For $\Omega < 10\,\mathrm{rad/s}$ the measured background was irreproducible and changed from run to run, preventing correct calibration of the device. Further investigation showed that the too large and irreproducible values of the background arose from a slight misalignment of the torque meter rotation axis with the disk and motor shafts. Since a large volume of fluid is being driven by a large and heavy dc motor, slight misalignments between the axes are not surprising. Moreover, the shaft attached to the spinning disk undergoes a slight nutation which is exaggerated by the height of couplers used to attach to the torque meter. The misalignment of the torque meter rotation axis and the motor shaft and the nutation of the disk shaft coupler causes small periodic variations in the measured torque, which if occurring singly can be filtered out from the measured signal. However, both these error mechanisms exist and in unison couple nonlinearly to produce a dc offset in the measured torque and cannot be filtered out. Hence the background signal measured is a sum of the friction in the bearings and the dc offset caused by the misalignment. We conclude that Γ_{err} consists of terms due to both the frictional losses and misalignment errors. In order to perform precise measurements at low frequencies and extend the range of the torque meter, the friction in both ball bearings and seals and misalignment had to be minimized. Two different seals were used to prevent water leakage from the ball bearings: at the bottom motor driving shaft the rotating SS-R00 John crane-type R00, AES P08, wave spring design, balanced end-face mechanical seal with guaranteed limited mechanical friction and at the top motor driving shaft the oil seal CR14223 with low mechanical friction from CR Services Co. High-precision machining and low-friction ball bearings and seals help alleviate the first problem.

To minimize the errors of the second kind the following modifications were made. Traditionally, soft helical spring couplers have been used as a solution to slight misalignment between two axes. Attaching spring couplers in our system caused the measured torque to oscillate at particular drive frequencies due to unavoidable nonlinear resonances. For accurate calibration the torque meter

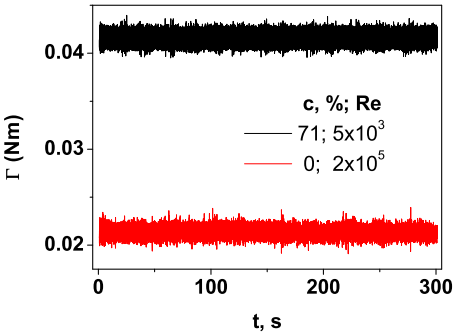

FIG. 2. Time series of torque $\Gamma(t)$ in the constant Ω forcing regime for (a) water at $T = 20.3\,^{\circ}\mathrm{C}$ ($\eta =$ 1 m Nm) and $\mathrm{Re} = 2 \times 10^5$ and (b) water-glycerol solution of $c = 71$ wt. % glycerol at $T = 21.2\,^{\circ}\mathrm{C}$ ($\eta =$ 21.5 m Nm) and $\mathrm{Re} = 5 \times 10^3$. The data acquisition rate is 100 Hz for both time series. Only a part of the data is shown.

rotation axis was precisely aligned with that of the disk shaft by attaching the former to a two-axis rotation stage attached to an XY translation stage. This configuration allowed enough degrees of freedom to align both the position and the angle of the torque meter. The radius of the disk shaft was 12.5 mm, while that of the torque meter was 3.15 mm. The coupler from the disk to the torque meter was machined out of aluminum and was tapered down, being wide (31 mm) at the bottom and narrow at the top (9.5 mm). This coupler design lowered its center of mass considerably and reduced nutation errors. At the top of the coupler a narrow notch (8 mm wide) was machined, into which the corresponding protrusion from the torque meter fit in precisely, analogous to a flat head screwdriver and screw. This arrangement minimized bending torques between the torque meter and the disk shaft, but caused a small mismatch in the shaft angles between the torque meter and the dc motor. The centers of the motor and torque meter were aligned by placing the former on an XY translation stage while errors due to angle misalignment were minimized by connecting the motor and torque meter with a two-arm connector which allowed two extra degrees of freedom. After these modifications the background dc signal was stable to within 0.2 m Nm, close to the precision allowed by the instrument. We also observed that at a low rotation speed the background torque does indeed increase due to a persistent misalignment owing to a nutation of the disk shaft coupler (this occurs because the shaft is not perfectly aligned with gravity). After the correct background subtraction, the measured torque is precise within 1 m Nm due to any misalignment errors. The final measured torque was filtered first by a 2-Hz low-pass filter to remove the PID signal and second by a notch filter to remove the drive frequency. Even after the careful alignment and measurement of the background torque, small deviations from the scaling dependence were observed for low rotation speeds. This stems from the fact that the background signal, specifically, the nonlinear interaction between the disk shaft and motor shaft, is modified in the presence of fluid that is impossible to estimate; measurements below 20 rpm ($\sim$2 rad/s) were unreliable and discarded.

The measurements of the torque fluctuations were conducted at constant rotation rates of the disk Ω through feedback control via optical encoders. A time series of the torque measurements at a constant Ω was used to test the stability of the measurements via deviation of $\bar{\Gamma}$ from its constant value. The degree of $\bar{\Gamma}$ of long-term stability for two data sets for the glycerol-water solution with $c = 71$ wt. % glycerol at $\mathrm{Re} = 5 \times 10^3$ and water at $\mathrm{Re} = 2 \times 10^5$ is presented in Fig. 2.

Water and water-glycerol solutions of different concentrations, different temperatures, and hence different dynamic viscosities η were used as the working Newtonian fluids. The water-glycerol solutions contained $c = 0$, 32, and 71 wt. % glycerol concentrations and temperatures $T = 20.3\,^{\circ}\mathrm{C}$, $20.0\,^{\circ}\mathrm{C}$, and $21.2\,^{\circ}\mathrm{C}$, respectively, were used, which correspond to the dynamic viscosities $\eta = 1$, 4.5, and 21.5 mPa s obtained via rheological measurements.

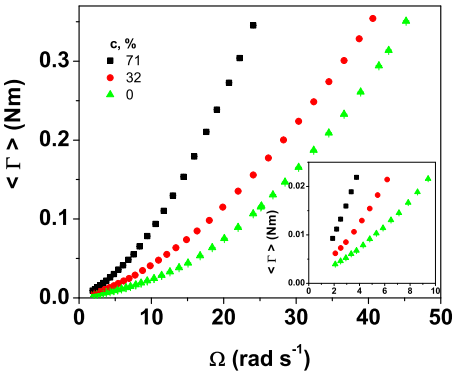

FIG. 3. Average torques $\bar{\Gamma}$ as a function of Ω for three water-glycerol solutions are shown. Error bars are smaller than the symbols.

Azimuthal $V_\theta(r,z,t)$ and axial $V_z(r,z,t)$ velocity profiles along radial and axial directions were measured by LDV including a two-component DANTEC FiberFlow fiber-based flow probe, transmitter, Coherent Innova 70 Ar-ion laser, and BSA-F30 Flow Processor. Two pairs of beams (488 and 514.4 nm) from the flow probe were focused onto a small sample volume of fluid of $0.1 \times 0.1 \times 2$ mm^3 that had been previously seeded with 20-μm polyamide seeding particles (from DANTEC). The fiber flow probe was mounted on vertical and horizontal translation stages to scan an area of 12 (r axis) $\times$ 11 cm^2 (z axis) in a vertical plane through the center of the rotating disk in steps of 5 and 10 mm, respectively. As a result, $V_\theta(r,z,t)$ and $V_z(r,z,t)$ velocity profiles were measured. The light reflected by the seeding particles was collected at an average rate of 100 Hz and approximately 10^4 data points were obtained at each spatial location for which the mean velocities were calculated. To better qualitatively understand the flow structure the streak movie visualization in the plane along the cell diameter at various flow parameters was also carried out.

III. RESULTS

A. Friction coefficient C_f as a function of Re

A common way to characterize the flow is through the dependence of the average torque $\bar{\Gamma}$ on the angular velocity Ω (or $\omega = 60\Omega/2\pi$ rpm) as shown in Fig. 3 for three water-glycerol solutions (and at different temperatures) over a wide range of Ω from about 2 up to 45 rad/s (or ω from about 20 up to 450 rpm). In the inset in Fig. 3, the data of $\bar{\Gamma}$ are shown for small values with higher resolution to highlight that all three curves would intersect the vertical axis at $\bar{\Gamma} \approx 0.2$ m Nm when extended down to $\Omega \to 0$, close to the torque meter resolution.

The same data ($\bar{\Gamma}$ as a function of Ω) is shown in nondimensional form in Fig. 4 as the friction coefficient $C_f = 2\bar{\Gamma}/\rho\Omega^2 R^5$ versus Re, in the laminar regime and further in a transitional regime toward turbulence. We were not able to reach the turbulent regime because the resulting torques generated would be beyond the upper limit of the high-precision torque meter. In the laminar regime, we found a well-defined scaling relation with a fit of $C_f = 1.17(\pm 0.03)\mathrm{Re}^{-0.46\pm0.003}$, shown in the inset in Fig. 4, in fair agreement with the von Kármán solution obtained for an infinite, smooth, unshrouded rotating disk [see Eq. (1) and Refs. [1–3]].

The dependence of the ratio of the rms torque fluctuations to the average torque $\Gamma_{\mathrm{rms}}/\bar{\Gamma}$ on Re is shown in Fig. 5; the normalized torque fluctuations saturate at higher Re and increase with decreasing Re due to the growing contribution of instrumentation noise to the measured torque at lower rotation speeds, which is probably caused by misalignment which remains in the limit of $\omega \to 0$ interacting with PID of the motor speed regulation.

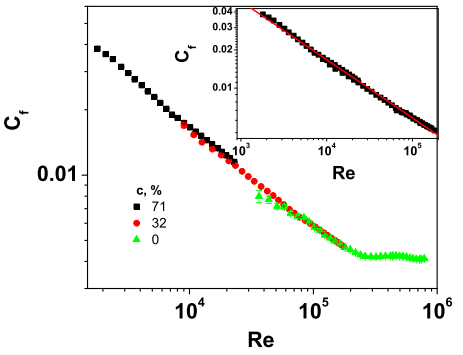

FIG. 4. Friction coefficients C_f as a function of Re for three water-glycerol solutions are presented together with error bars, which are smaller than the symbol sizes. The inset shows C_f versus Re of only a laminar flow part. In each data set the first 3–4 points at smaller values of Re deviating from the main dependence were omitted. A solid line is the fit to the whole data set.

B. Radial and axial profiles of the azimuthal and axial average velocity components

Azimuthal and axial velocity components at different radial and axial positions in a laminar flow regime at $\omega = 300$ rpm (or $\Omega = 10\pi$ rad/s) in a water-glycerol solution at 71 wt. % glycerol concentration and at $T = 21.2\,^{\circ}$C, corresponding to $\mathrm{Re} = 2.55 \times 10^4$, were measured by a two-component LDV in a vertical plane through the rotation axis. Figure 6(a) shows radial profiles of the averaged azimuthal velocity component $V_\theta(r)$ at 11 axial positions. Close to the rotation axis, $V_\theta(r)$ depends linearly on r linear for all axial positions. An example of such a dependence at $z = 3$ cm is shown in the inset of Fig. 6(b) together with the fit at $r \leqslant 35$ mm. The fit provides the value of the slope V_θ/r, which is the angular velocity of the rotating core of the flow. The values of normalized core rotating velocity $V_\theta/r\Omega$ are presented in Fig. 6(b) for all 11 axial positions. From linear fits we find that $V_\theta/r\Omega = 0.219 \pm 0.001$ for $z \leqslant 4$ cm and then drops steeply down to 0.193 ± 0.003 up to $z = 11$ cm, as shown in Fig. 6(b). In Fig. 7 the same data as a function of r/R for four axial positions close to the rotating disk are shown. A large scatter around the average value of the normalized angular core velocity is a result of the normalization, where the error grows as $1/r$ at $r \to 0$. From the normalized core angular velocity we also determine the size of the rotating core to be of the order $r_0/R \simeq 0.25$ for four axial locations. For the axial locations far away from the rotating disk both the core size and core angular velocity are reduced in magnitude. Thus, the normalized radial profile of the azimuthal velocity components clearly indicate a core rigid body rotation (see also movie2 and movie6 at different flow parameters in Ref. [14]). The radial profile of the axial component of the

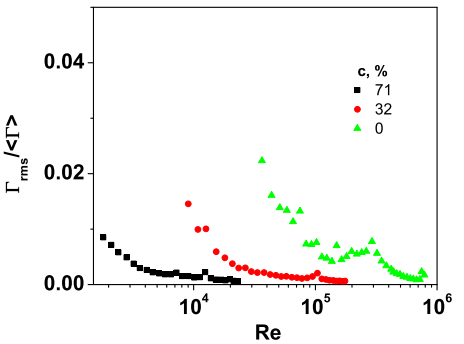

FIG. 5. Dependence of $\Gamma_{\mathrm{rms}}/\bar{\Gamma}$ on Re in the laminar regime for three water-glycerol solutions.

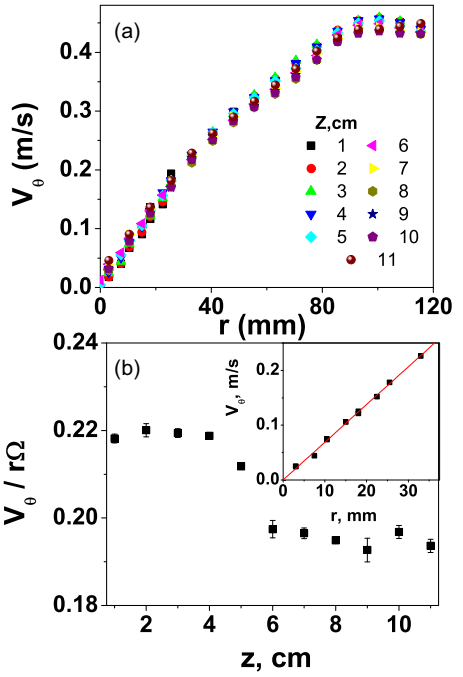

FIG. 6. (a) Radial profiles of V_θ for 11 axial locations and (b) normalized $V_\theta/r\Omega$ in the rotating core as a function of z. The inset shows an example of the radial profile of V_θ in the rotating core for $z = 3$ cm; a solid line is the fit.

velocity in the laminar regime V_z shows an almost linear growth with r from 0 at the center up to approximately $R/2$ for all axial distances from the rotating disk explored in the experiment and then a slower than linear dependence from $R/2$ up to R with a weak dependence on the axial location (see Fig. 8 and movie1, movie3, movie4, and movie5 at different flow parameters in Ref. [14]). Both particle image velocimetry and streak images reveal a complicated flow structure due to closely located lateral walls (the small-aspect-ratio cell) and the small gap between the disk rim and the lateral wall. From the steak images presented as six movies for different flow parameters and the LDV the following qualitative structure can be inferred.

Close to the spinning disk surface there exists a thin boundary layer, where the angular velocity drops steeply from Ω to $\sim 0.22\Omega$ right outside it, which cannot be imaged precisely given our current

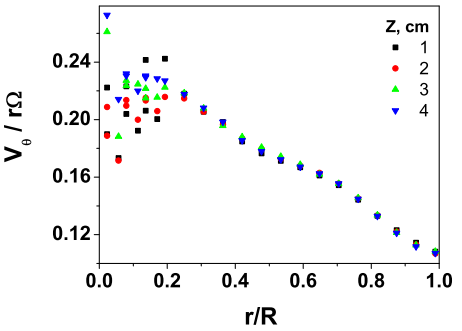

FIG. 7. Normalized radial profiles of $V_\theta/r\Omega$ vs r/R for four axial locations close to the rotating disk.

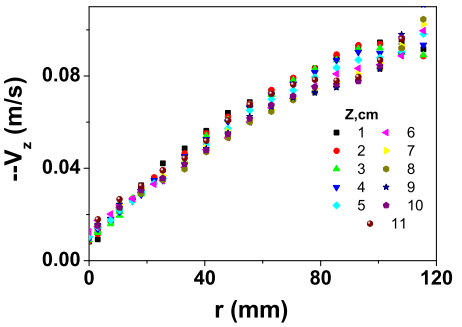

FIG. 8. Radial profiles of V_z for 11 axial locations.

optical setup. Outside this boundary layer we can identify three distinct flow regions. (i) In the center of the cylinder there is a core flow up to $r_0/R \simeq 0.25$, where the fluid spins as a solid body with angular velocity $\sim 0.22\Omega$ (movie6 at $\mathrm{Re} = 8.95 \times 10^4$). The core flow extends from the boundary layer down to the stationary disk, tapering down in radius until it almost becomes zero. From Fig. 6 one can see that the core velocity decreases to $\sim 0.19\Omega$ at $z = 6$ cm up to $z = 11$ cm and finally becomes zero at the stationary disk. At low rotation speed (less than 100 rpm), the core is unstable to gentle undulations and also shows an alternating structure between core rotation and axial from toward the spinning disk (movie2 at $\mathrm{Re} = 4.25 \times 10^3$). (ii) An outer flow region extends from the core boundary to almost the walls of the container. This region also extends from the boundary layer to the stationary disk, but in the bulk of the flow the angular velocity steadily drops from the core rotation velocity to $\sim 0.10\Omega$ at $r_0/R \simeq 1$. Thus we identify a strong shear layer between a solid spinning core and outer flow region. While it is not possible to extract radial velocity profiles using our current setup, streak images help to identify strong radial inflow in the outer region. The axial flow in both these regions is weak, with velocity ~ 5 times smaller than the azimuthal component. (iii) Finally, there is a thin recirculating gap region between the outflow region and the walls of the container where fluid thrown out at the disk due to centrifugal forces is sucked back into the bulk (see the movies in [14]). The overall picture of the flow that emerges is the same. There is a central solid rotating core that extends from the boundary layer to the bottom, outside of which fluid is drawn radially inward toward the core (there is weak axial flow within the core also) and axially toward the disk and then ejected from the disk surface due to centrifugal forces into the gap region from which it recirculates back into the bulk.

Thus the flow is more complicated than predicted theoretically in both the Batchelor and Stewartson cases due to the strong influence of the lateral wall and the suction in the gap region. However, at sufficiently large Re it strongly resembles the Batchelor solution.

IV. DISCUSSION AND CONCLUSIONS

The main result of this work is the scaling relation of C_f with Re with an exponent and coefficient that deviate slightly from the prediction made for an infinite, smooth, rotating, and unshrouded disk [1–3]. The question remains whether the disagreement with the theoretical prediction is due to the difference between the assumptions of the theory about an infinite and unshrouded rotating disk and the experimental finite and shrouded one or is caused by the background friction losses and misalignment errors leading to a distortion of the expected dependence, in particular at lower rotation speeds.

In this section we estimate the experimental errors and gauge whether they can explain the deviation of the scaling of the friction coefficient. The total measured torque consists of a term from the signal Γ_{sig} and terms that come from the background losses and misalignment errors Γ_{err}. Then the total friction coefficient can be written as $C_f \equiv 2(\Gamma_{\mathrm{sig}} + \Gamma_{\mathrm{err}})\rho/R\eta^2\mathrm{Re}^2 = 1.935\,\mathrm{Re}^{-0.5}$.

A significant effect of $\Gamma_{\rm err}$ on the scaling may be expected at $\Gamma_{\rm err} \geqslant \Gamma_{\rm sig}$. Then one can estimate the value of $\Gamma_{\rm err}$ above which it affects the scaling relation $\Gamma_{\rm err} \geqslant (1.935/2\rho)R\eta^2{\rm Re}^{3/2}$, which gives for water $\Gamma_{\rm err} \sim 10^{-10}{\rm Re}^{3/2}$. At ${\rm Re} = 10^6$ one gets $\Gamma_{\rm err} \sim 0.1$ Nm, whereas for ${\rm Re} = 3 \times 10^4$ the lowest value for water reached in the experiment, it is $\Gamma_{\rm err} \sim 1$ m Nm. As one can see from the plot in Fig. 4, at ${\rm Re} \simeq 3 \times 10^4$ the deviations from the scaling toward smaller values of Γ are visible. That is the reason for omitting the first few data points in each data set at the lowest Re to get the fits (compare the main plot with the inset in Fig. 4). Thus the background errors intend to reduce the absolute value of the scaling exponent. So one can conclude that the small deviation from the theoretical prediction in the value of the scaling exponent found in the experimental data may be at least partially explained by $\Gamma_{\rm err}$.

On the other hand, the LDV measurements of the azimuthal $V_\theta(r,z,t)$ and axial $V_z(r,z,t)$ velocity profiles along radial and axial directions reveal that the flow core rotates at $V_\theta/r\Omega \simeq 0.22$ up to $z = 4$ cm from the rotating disk and up to $r_0/R \simeq 0.25$ in the radial direction in spite of the small aspect ratio of the vessel. The flow core angular velocity should be compared with $\sim 0.3\Omega$ found from the Batchelor solution [4]. Thus the friction coefficient shows scaling close to that obtained from the von Kármán exact similarity solution [1], but the observed rotating core provides evidence of the Batchelor-like solution [4] different from the von Kármán [1] or Stewartson [5] one. This probably means that the dependence of C_f on Re is not sufficiently sensitive to the flow structure; the result is worth verifying by numerical simulations.

ACKNOWLEDGMENTS

This work was partially supported by the Israel Science Foundation (ISF; Grant No. # 882/15).

[1] T. von Kármán, Uber laminare und turbulente reibung, Z. Angew. Math. Mech. **1**, 233 (1921).
[2] W. G. Cochran, The flow due to a rotating disk, Proc. Camb. Philos. Soc. **30**, 365 (1934).
[3] M. H. Rogers and G. N. Lance, The rotationally symmetric flow of a viscous fluid in the presence of an infinite rotating disk, J. Fluid Mech. **7**, 617 (1960).
[4] G. K. Batchelor, Note on a class of solutions of the Navier-Stokes equations representing steady rotationally symmetric flow, Q. J. Mech. Appl. Math. **4**, 29 (1951).
[5] K. Stewartson, On the flow between two rotating coaxial disks, Proc. Camb. Philos. Soc. **49**, 333 (1953).
[6] P. J. Zandbergen and D. Dijkstra, von Kármán swirling flows, Annu. Rev. Fluid Mech. **19**, 465 (1987).
[7] G. L. Mellor, P. J. Chapple, and V. K. Stokes, On the flow between a rotating and a stationary disk, J. Fluid Mech. **31**, 95 (1968).
[8] K. G. Picha and E. R. G. Eckert, in *Proceedings of the Third U.S. National Congress on Applied Mechanics*, edited by R. M. Haythornthwaite *et al.* (ASME, New York, 1958), p. 791.
[9] F. Bien and S. S. Penner, Velocity profiles in steady and unsteady rotating flows for a finite cylindrical geometry, Phys. Fluids **13**, 1665 (1970).
[10] D. Dijkstra and G. J. F. van Heijst, The flow between two finite rotating disks enclosed by a cylinder, J. Fluid Mech. **128**, 123 (1983).
[11] J. F. Brady and L. Durlofsky, On rotating disk flow, J. Fluid Mech. **175**, 363 (1983).
[12] A. Z. Szeri, S. J. Schneider, F. Labbe, and H. N. Kaufman, Flow between rotating disks, Part 1. Basic flow, J. Fluid Mech. **134**, 103 (1983).
[13] H. Schlichting and K. Gersten, *Boundary Layer Theory* (McGraw-Hill, New York, 2000).
[14] See Supplemental Material at http://link.aps.org/supplemental/10.1103/PhysRevFluids.3.014102 for movies.